Truncation effect reduction for fast iterative reconstruction in cone-beam CT

Sorapong Aootaphao (aootaphao@gmail.com)
Faculty of Medicine, Price of Songkla University, Songkhla

Saowapak Thongvigitmanee
Medical Imaging System Research Team, Assistive Technology and Medical Devices Research Center, National Science and Technology Development Agency, Pathum Thani

Puttisak Puttawibul
Faculty of Medicine, Price of Songkla University, Songkhla

Pairash Thajchayapong
National Science and Technology Development Agency

Research Article

Keywords: cone-beam CT, iterative reconstruction, x-ray scattering reduction, metal artifact reduction, truncation effect reduction and artifact reduction in CBCT imaging

Posted Date: September 15th, 2021

DOI: https://doi.org/10.21203/rs.3.rs-900212/v1

Truncation effect reduction for fast iterative reconstruction in cone-beam CT

Sorapong Aootaphao [1, 2 *], Saowapak S. Thongvigitmanee [2], Puttisak Puttawibul [1] and Pairash Thajchayapong [3]

Abstract

Background: Iterative reconstruction for cone-beam computed tomography (CBCT) has been applied to improve image quality and reduce radiation dose. In a case where an object is larger than a flat panel detector, most CBCT images contain truncated data or incomplete projections, which degrade image quality. In this work, we propose the truncation effect reduction for fast iterative reconstruction in CBCT imaging inside the field of view (FOV).

Methods: The volume matrix size of FOV and the height of projection images were extrapolated to a suitable size. These extended projections were reconstructed by fast iterative reconstruction. Moreover, a smoothing parameter for noise regularization in iterative reconstruction was also modified to reduce the accumulated error while processing. The proposed work was evaluated by image quality measurements and compared with the conventional filtered back projection (FBP) method. To validate the proposed method, we used a head phantom for evaluation and tested on real human head data.

Results: In the experimental results, the reconstructed images from the head phantom can be enhanced apparently. In addition, fast iteration reconstruction can be run continuously while remaining the consistent mean-percentage-error (MPE) value with a large number of iterations. The CNR of the soft-tissue images was improved by the increased contrast and the decreased noise. Visualization of low contrast in the ventricle and soft-tissue images can be observed much clearer compared to those from FBP using the same effective radiation dose of 5 mGy.

Conclusions: Our proposed work has satisfactory performance to reduce the truncation effect, especially inside the FOV with better image quality for soft-tissue imaging. The convergence of fast iterative reconstruction tends to be stable for many iterations.

Keywords: cone-beam CT, iterative reconstruction, x-ray scattering reduction, metal artifact reduction, truncation effect reduction and artifact reduction in CBCT imaging

Background

Cone-beam computed tomography (CBCT) technology, which uses the modern equipment of an x-ray source and a flat-panel detector (FPD), is widely used due to its small machine size, large field of view (FOV), and low radiation dose [1-3]. Most of this technology is applied for diagnosis and treatment planning, such as dental, maxillofacial, orthopaedic, and breast-cancer specimen imaging [4, 5]. The quality of images reconstructed from CBCT is often deteriorated by many causes, such as X-ray scattering, beam hardening, metal artifact, and truncation artifact [4, 6-11]. Specifically, truncated data or incomplete projection images are often noticeable when an object is larger than a detector active area and thus directly affecting image quality and reconstruction. As a result, hard-tissue and soft-tissue imaging cannot be clearly visualized in the reconstructed images. However, good image quality in CBCT imaging is still required and important for diagnosis of the diseases. Generally, artifacts from the truncation effects are easy to handle with filtered back projection (FBP) reconstruction but not iterative reconstruction (IR). Compared to FBP, IR is more susceptible to incomplete data due to accumulation of errors leading to the artifacts.

Many researchers have studied and developed truncation effect reduction in CBCT imaging. Ohnesorge *et al* 2000 [6] estimated the lost data in projection images using symmetric mirroring extrapolation, and Hsieh *et al* 2004 [7] approximated the lost data with extrapolation using the fitted water cylinder. Both techniques extended projection images and synthesized new information that filled truncated projection images during the convolution process in FBP. Maltz *et al* 2007 [12] proposed CT truncation artifact removal using water-

*Correspondence: aootaphao@gmail.com
[1] Faculty of Medicine, Price of Songkla University, Songkhla, Thailand.
[2] Medical Imaging System Research Team, Assistive Technology and Medical Devices Research Center, National Science and Technology Development Agency, Pathum Thani, Thailand.

equivalent thickness. This method assumed that the outline of large body parts could be roughly approximated as an ellipse to predict and estimate the lost data in the truncated or incomplete projection images. Another research published by Dang *et al* 2017 [13] attempted to mitigate the truncation effect in iterative reconstruction by a downsampling method and an extension of FOV, but that was applied only on the extended FOV in the axial plane of the reconstructed image. In fact, the truncation artifact can appear not only on the axial plane but also on the sagittal plane of the FOV, i.e., the upper and lower parts of the head.

Herein, we propose a novel truncation reduction method for CBCT the truncation effect reduction in CBCT imaging. Our proposed method expands the size of the FOV and extrapolates the height of projection images including an image smoothing parameter for noise regularization in reconstruction. Here, fast iterative reconstruction employs the modified convex algorithm with additional penalized likelihood estimation called the PL-C algorithm [14-18]. Then, the PL-C is additionally modified to accelerate the convergence by using acceleration techniques [19-21]. To validate the proposed work, the proposed method was experimentally validated with an anamorphic head phantom and a real human head. The validation results were compared against those from FBP [22, 23].

Methods

A CBCT scanner prototype was installed on a benchtop system as shown in Fig. 1. A system consisted of an x-ray source, a rotation stage using a stepping motor, and a flat panel detector based on amorphous silicon thin-film transistors. The x-ray source has a maximum power of 5 kW; tube potential of 50-120 kVp, a focal spot size of 0.6 mm; a rotating anode, and a 15-degree target angle. The detector has the size of 40 cm x 30 cm and the pixel pitch of 0.194 mm. The distance from a source to a detector (DSD) in this system is 950 mm and the distance from a source to an object (DSO) is 500 mm. The center of the x-ray is aligned toward the center of the flat panel detector (FPD) and the FOV. The projection dataset was acquired using 100 kVp, 7 mA, and 40.32 mAs. The computed tomography dose index (CTDI) value measured in this system for scanning was 5 mGy. An anamorphic head phantom used for verification of the algorithm and image quality was the PH3 angiographic CT head phantom (Kyoto Kagaku, Japan) placed at the rotation stage. Moreover, we also analyzed the proposed work with one anonymous human head data set, which was retrospective and used for different purposes. All of the proposed work used the computer (processor of Core-i7-9700 CPU at 3.0 GHz, RAM of 16 GB) for developing the algorithm and was implemented on a graphic processing unit (GPU) card (GeForce RTX2070, NVIDIA) with a CUDA library.

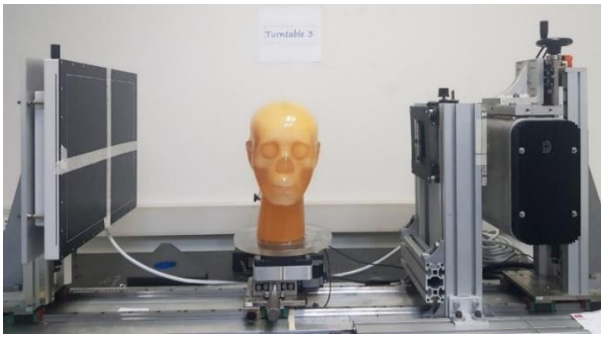

Fig. 1 The CBCT scanner prototype on a benchtop system

An anamorphic head phantom was scanned by the CBCT scanner prototype. In CBCT imaging, we can perform a few processes sequentially, such as the scatter correction, fast iterative reconstruction with the proposed truncation effect reduction, and image quality evaluation. These processes can be described by the flowchart as shown in Fig. 2. The in-house scatter correction algorithm [24, 25] was applied to projection data before reconstruction to accurately estimate the x-ray scatters.

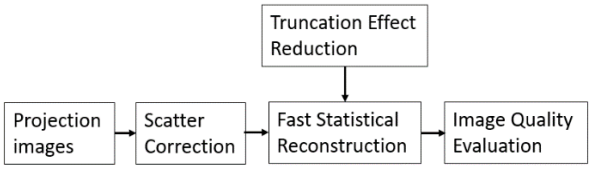

Fig. 2 The overall process of the proposed reconstruction

Fast Iterative Reconstruction

Statistical iterative reconstruction is based on maximum likelihood estimation with the convex function [15-18]. The maximum likelihood function $L(\mu)$ estimates the linear attenuation coefficient in 3D cross-section or volume images from projection images. The objective function of the maximum likelihood algorithm is modified by adding a penalty function to regularize noise. Thus, the estimate of the attenuation is obtained by maximizing the objective function as follows:

$$\hat{\mu} = \arg\max_{\mu \geq 0} \Phi(\mu) \tag{1}$$

where the objection function Φ is given by

$$\Phi(\mu) = L(\mu) - \beta R(\mu) \tag{2}$$

where β is a parameter for smoothness control, $R(\mu)$ is the roughness penalty based on a potential function ψ that uses the huber function [14, 17] for edge-preserving.

$$\psi = \begin{cases} \frac{\mu^2}{2}, & |\mu| \le \delta \\ |\mu| - \frac{\delta^2}{2}, & |\mu| > \delta \end{cases}$$

where δ controls the level of edge preservation. The PL-C algorithm [17, 18] is used to calculate the attenuation coefficient in equation (1). Thus, the update Δ of the attenuation coefficient μ_j at iteration n+1 is calculated as follows:

$$\mu_j^{n+1} = \mu_j^n + \Delta$$

Iterative reconstruction is well-known for taking a long processing time. Thus, several approaches have been investigated to reduce the processing time. One conventional acceleration technique is to divide the projection images into ordered subsets (OS) [16, 17] to improve the reconstruction speed. Each ordered subset of projections is performed in subiterations for reconstruction. All of subiterations is achieved to one iteration and update of the volume. Therefore, the number of forward and backward operations per update in each iteration is reduced. Yet the convergence is still slow. Another acceleration technique proposed by Kim and Fessler 2013 [19], and Kim *et al* 2015 [20], modified the momentum between the last and current updates to achieve a faster convergence. Such a method is known as Nesterov (NES) [21] acceleration, which can be explained in the equation below:

$$\mu_j^{n+1} = \left(1 - \frac{1}{t}\right) z + \frac{1}{t}(\mu^0 - v)/2 \qquad (3)$$

where

$$z = \mu_j^n + \Delta$$

$$v = v + t \cdot \Delta$$

$$t = (1 + \sqrt{1 + 4t^2})/2$$

where n is the number of iterations, z is the current image estimation, v is the summation of the momentum from all subiterations, and t is the momentum weight that linearly increases in each subiteration. The parameter of μ^0 can be initialized with arbitrary values or FBP. In this work, iterative reconstruction with both acceleration techniques was performed for *n* iterations and *m* subsets denoted by OS-*m* and NES-*m*, respectively.

Truncation effect reduction

Incomplete projection images or truncated data are often observed while scanning an object that is larger than the detector area. Some data on the peripheral sides may not appear in some projections. In addition, the longitudinal areas of a real human head (along the upper and lower parts) or a head phantom in projection images are usually truncated in most cases as shown in Fig. 3. Thus, truncated data around projection images are still the main cause of the degraded image quality, as it generates new artifacts and directly affects 3D reconstructed images.

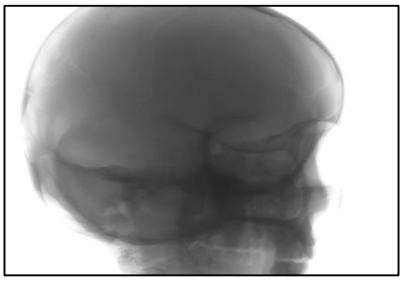

Fig. 3 An example of truncation data providing an incomplete projection image in the longitudinal areas of a head phantom

A conventional technique for truncation effect mitigation in iterative reconstruction is to compensate error data causing large differences between incomplete measurements and calculated forward projections. The compensation extends the matrix volume size of the FOV in the X-Y or axial plane as shown in Fig. 4. However, this technique is insufficient due to the remaining accumulated error in the regions of the Y-Z or longitudinal plane [13] in the FOV. Therefore, in this paper, we propose the extension of the matrix volume size, especially in the longitudinal plane outside the FOV as shown in Fig. 5. In addition, projection images are modified by extrapolating along the longitudinal planes with the extended height that can be simply calculated as follows:

$$\acute{d} = \left(h + \acute{h}\right)\frac{DSD}{DSO} - d \qquad (4)$$

where d is the height of the detector, $\acute{d}$ is the extended height, h is the height of the FOV, and $\acute{h}$ is the extended height. Due to difficulty in simulating the actual information lost in truncated data, we selected the most probable data to use in $\acute{d}$ as data rows at the border of projection images. Therefore, the projection images were extrapolated by the last data rows as shown in Fig. 6. Moreover, we found that a smoothing parameter β in the iterative reconstruction could well tackle noise in the reconstructed images, but a large smoothing value may rapidly increase the accumulated error [19, 21, 26]. The accumulated error in each iteration is controlled by limiting β to not more than an expected constant value c based on acceptable image quality. Thus, the entire extended FOV and projection are performed with fast iteration reconstruction, and we define the reconstruction with different β values

outside the FOV. The smoothing parameter β outside the FOV is set to zero to avoid accumulated error while processing.

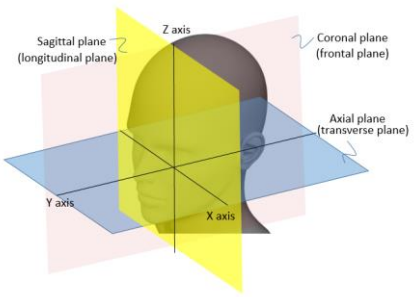

Fig. 4 Definition of imaging planes in the volume matrix of the FOV

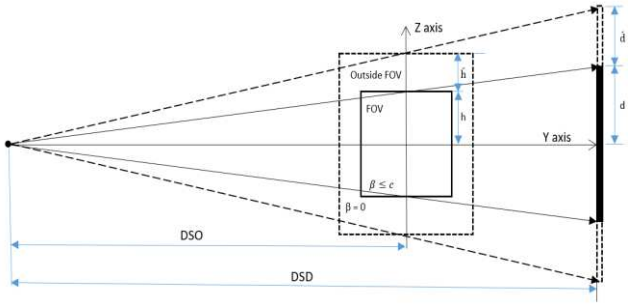

Fig. 5 The geometric system of extending the FOV in the Y-Z plane of the volume matrix and the height of detector

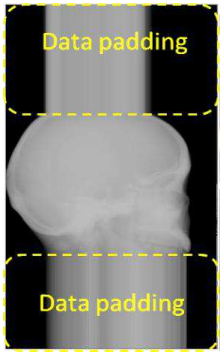

Fig. 6 Data extrapolation along the longitudinal plane in the projection image

Image Quality Evaluation

The head phantom was placed partially inside the FOV to simulate the truncation effect. The truncated data or incomplete projection images of the head phantom were acquired from the prototype. They were corrected for x-ray scattering [24, 25] and reconstructed by fast iterative reconstruction with the proposed truncation effect reduction to obtain the reconstructed images. In this case, we focused on certain slices of reconstructed images in the upper part inside the FOV because they tend to degrade easier than other slices.

Noise at the slices inside the FOV was measured with different matrix volume sizes in the Y-Z plane. In the performance measurements of convergence in iterative reconstruction with and without the proposed effect reduction, the mean-percentage-error (MPE) value was used inside the region of interest (ROI) in each iteration and normalized by the reconstruction image from OS-1 at 1000 iterations as follows:

$$\%MPE = \frac{100}{N} \times \sum \left(\frac{|\mu_{OS-1}^{1000} - \mu^{n}|}{\mu_{OS-1}^{1000}} \right) \quad (5)$$

where N is the total number of pixels inside the ROI, n is the number of iterations. Moreover, the contrast-to-noise ratio (CNR) value was used for image quality evaluation and comparison with FBP as follows:

$$CNR = \frac{M_x - M_b}{\sqrt{\sigma_x^2 - \sigma_b^2}} \quad (6)$$

where M_x is the average intensity in the ROI in the reconstructed images, M_b is the average intensity of the background, and σ_x and σ_b are the standard deviation of the ROI and background, respectively.

Results

The Truncation Effect Reduction

Figure 7 shows the results of the reconstructed images in the axial, sagittal and coronal planes with and without the proposed work. The PL-C algorithm with the accelerated techniques was applied for the reconstruction using β=150, δ = 0.00005, OS-10, and 20 iterations. The expected FOV has the volume matrix size of 400x400x324 voxels while the extended size contained 600x600x800 voxels with the voxel size of 0.5 mm. In the experiment, Fig. 7 (a)-(c) are the results of the reconstructed images without the proposed method. We found that many shades and streaks from the truncation effect were distinctly appeared in the entire reconstructed images showing in the axial, sagittal, and coronal planes. The results of the reconstructed image with the proposed method are shown in Fig. 7 (d)-(f). The red dash frames in Fig. 7 (d)-(f) represent the expected FOV, corresponding to the same area in Fig. 7 (a)-(c). The artifacts from truncation effect inside the FOV are apparently reduced although they still exist outside the FOV. Figure 8 shows the reconstructed images and the noise measurement with different extended sizes. In the experiment, the image size in the axial or X-Y plane was fixed at 600x600 voxels and the number of slices in the longitudinal or Y-Z plane was varied between 324 and 800 slices. The artifacts appeared in the slices are decreased when a number of slices are increased as shown in Fig. 8 (a)-(c).

In addition, noise from artifacts is continuously decreased until the algorithm is converged and consistent with the increased height of the FOV as shown in Fig. 8 (d). Hence, the consistent decreased noise can be the stopping criteria for the extended height of the FOV.

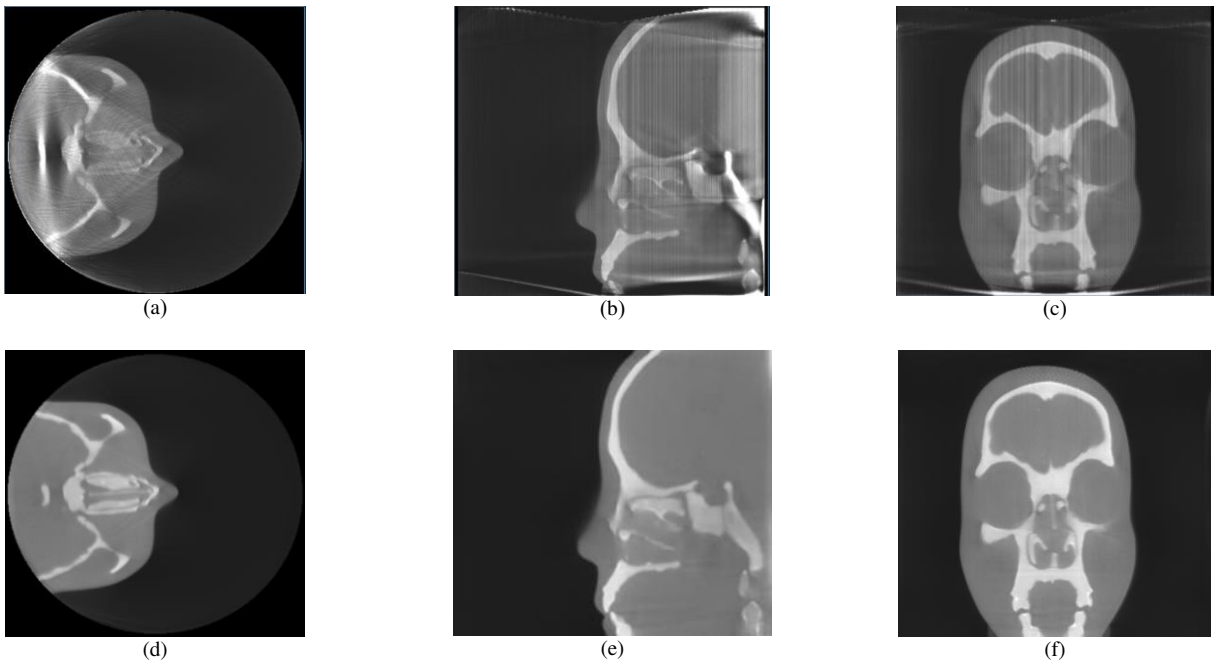

Fig. 7 Reconstructed images (1st row) without and (2nd row) with the proposed method using the anamorphic head phantom in **a** and **d** the axial planes, **b** and **e** the sagittal planes, and **c** and **f** the coronal planes, respectively

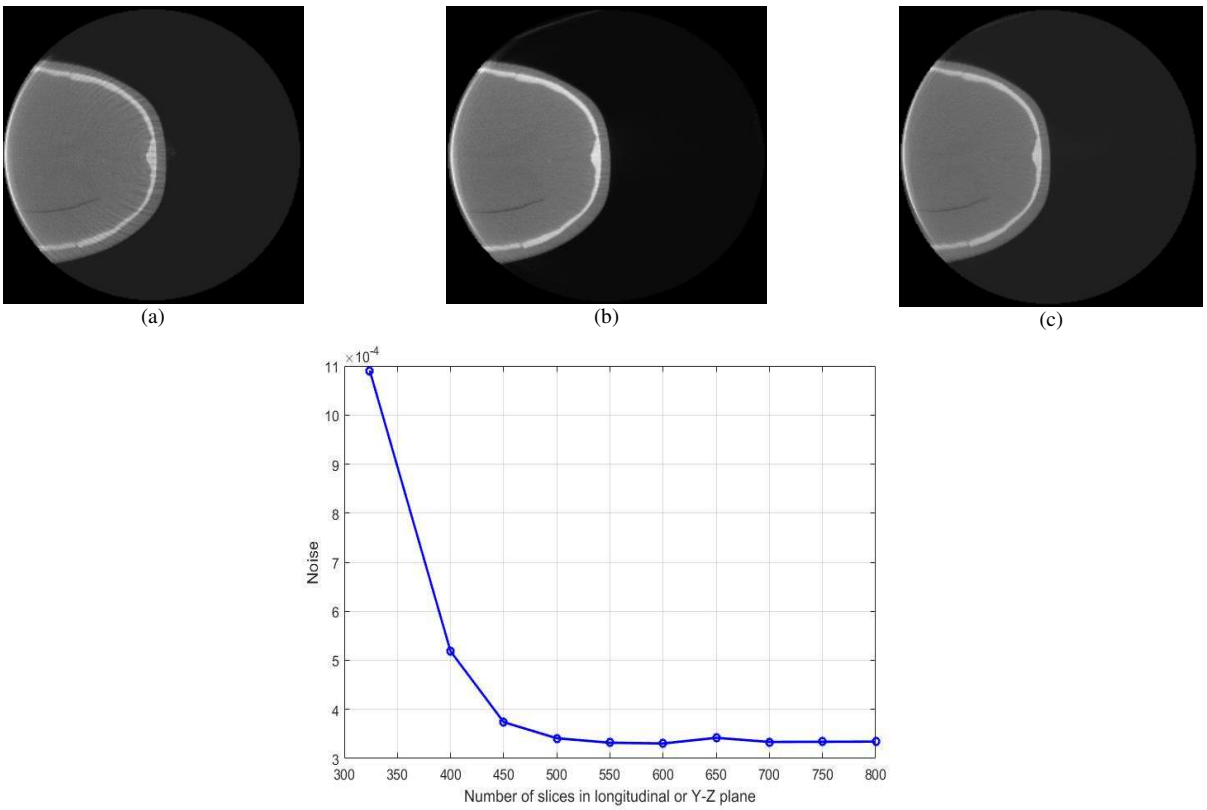

Fig. 8 The reconstructed images in the FOV **a** without extended height using 324 slices, **b** with extended height using 450 slices, **c** with extended height using 800 slices. **d** Noise against different numbers of slices in the extended FOV

Mean-Percentage-Error Evaluation

The MPE value was calculated from the reconstructed images in each iteration using equation (5). Reconstruction with and without the proposed work was fixed at β =150, δ = 0.00001, 1000 iterations and varied acceleration techniques as follows: OS-10 and NES-10. The results of MPE were plotted together in Fig. 9. We found that the MPE values of OS-10 and NES-10 without the reduction of truncation effect did not converge but kept increasing. On the contrary, the MPE values of both acceleration methods with the reduction of truncation effect showed a stable convergence at 100 iterations. Though, NES-10 seemed diverging a little after a certain iteration.

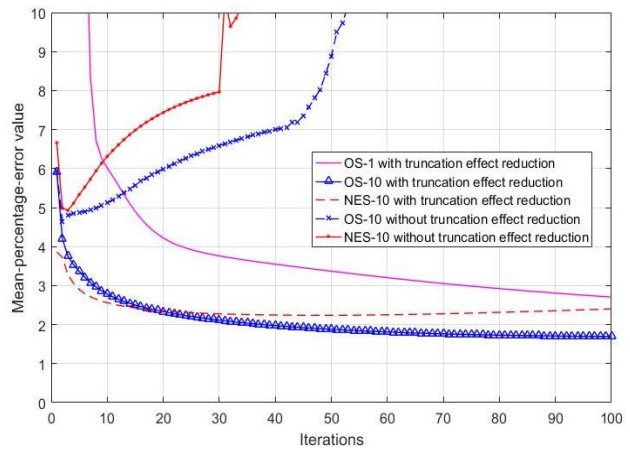

Fig. 9 MPE values using acceleration techniques against each iteration

The results with human head data

In the experimental results, the real human head data using CTDI of 5 mGy was tested with the proposed method. Figure 10 shows a comparison of the sagittal plane results of a human head between the FBP (using the hamming filter and the cut-off frequency of 0.65, 480x480x368 voxels) and the PL-C algorithm (using β=150, δ = 0.00001, OS-10, 20 iterations, 600x600x800 voxels) with and without the proposed truncation effect reduction. In the results of the PL-C algorithm without the truncation effect reduction, the red arrows indicated the artifacts around the truncated border of the images. But the artifacts in these areas from the proposed method can be reduced apparently as shown in Fig. 10 (c). Moreover, Fig. 11 shows the soft-tissue image results as compared with FBP. The CNR value on soft-tissue images with the ROI size of 20x20 pixels was evaluated against the background. The CNR from the PL-C algorithm with the proposed truncation effect reduction is significantly higher than that from others as shown in Table 1. The processing times of the FBP and PL-C algorithms were 10 sec and 4 min, respectively, but the PL-C algorithm with the truncation effect reduction used the longer processing time as 6 min. Moreover, we selected some slices of the ventricle-tissue images for comparison as the reconstructed images from FBP and PL-C algorithm with the proposed method were shown in Fig. 12. The ventricle in both brain images from the proposed method can be observed easier than that from FBP apparently as the red arrows indicated in the reconstructed images as shown in the second row of Fig. 12.

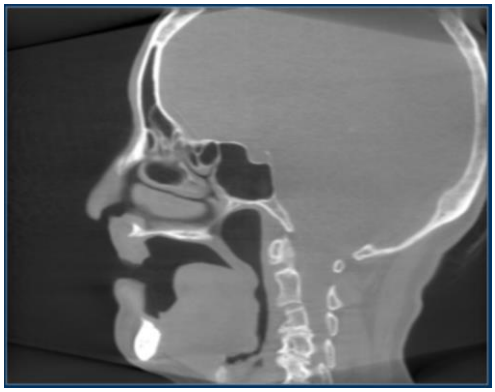

(a)

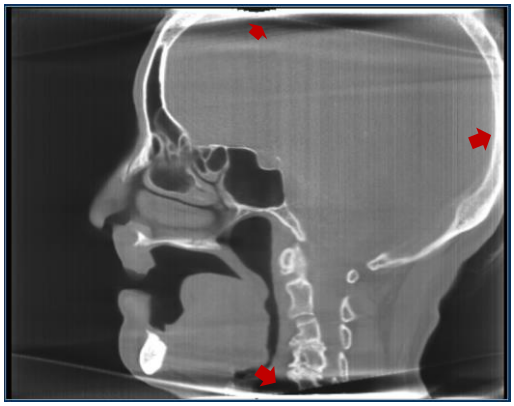

(b)

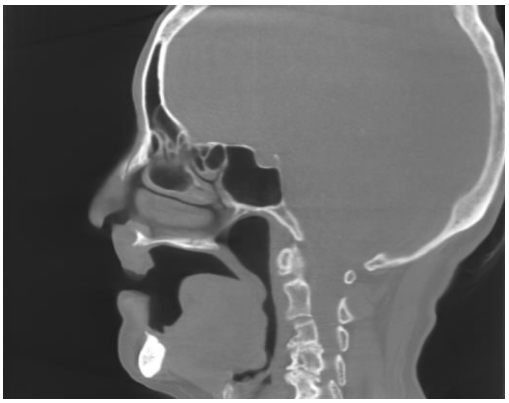

(c)

Fig. 10 The comparison of the sagittal plane results of a human head data with **a** FBP, **b** PL-C without truncation effect reduction where the red arrows indicated the artifacts at the truncated border of the image, and **c** PL-C with truncation effect reduction

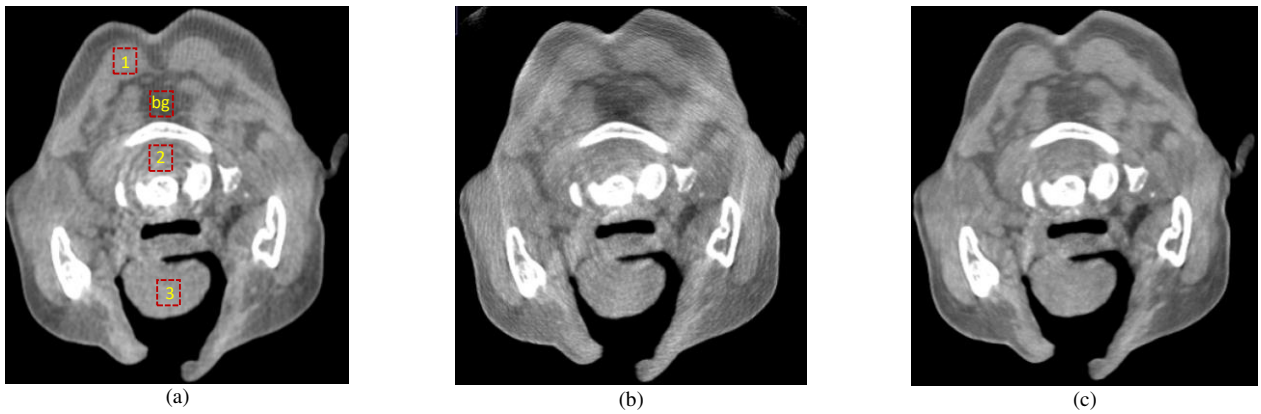

(a) (b) (c)

Fig. 11 The comparison of soft-tissue image results with **a** FBP, **b** PL-C without truncation effect reduction, and **c** PL-C with truncation effect reduction. Note that the CNR measurements were calculated at 3 red squared ROIs against the background

Table 1 Contrast to noise ratio comparison in the soft-tissue areas

	FBP	PL-C	PL-C with the proposed method
ROI#1	12	13	58
ROI#2	6	10	10
ROI#3	16	9	32

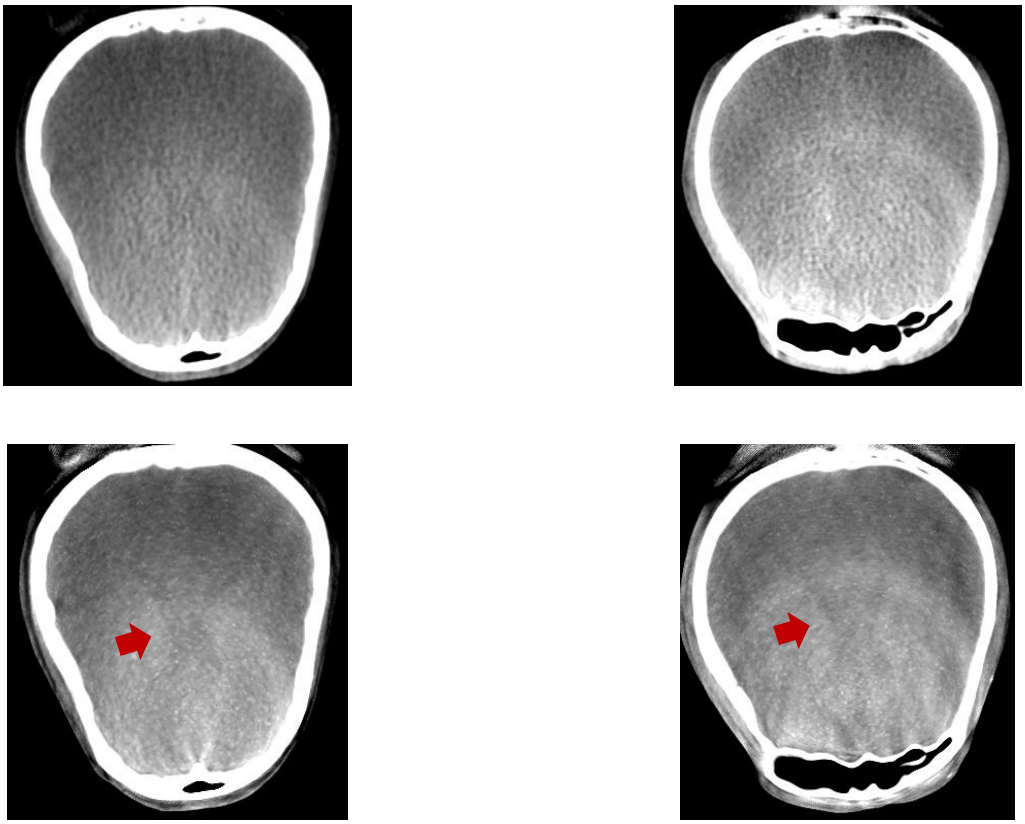

Fig. 12 The ventricle-tissue images from (1st row) FBP and (2nd row) the proposed method. Note that the ventricles are indicated by the red arrows

Discussion

Truncated data or incomplete projection images are obviously seen when an object is larger than a detector active area and the truncation artifacts are highly sensitive to iterative reconstruction. In this work, the size of FOV and the height of projection images were expanded using extrapolation and fast iterative reconstruction was performed by using the modified smoothing parameter to reduce the accumulated error. As seen in the reconstructed image of the head phantom and human head, the artifacts inside the FOV are effectively reduced. However, some artifacts are still noticeable outside the FOV because of inaccurate extrapolation and insufficient compensation in reconstruction. The smoothing parameter β helps the reduction of noise in imaging by varying the parameter value as the decreased noise in the reconstructed image is controlled by increasing the value β. Since the noise regularization using the smoothing parameter outside the FOV in the extended areas is out of interest, the penalty term in IR for noise reduction in equation (2) is ignored by letting β to be zero. The accumulated error of the reconstruction is well reduced. However, the accumulated error at the high iteration do not decrease because of no weight in the update term of IR, i.e., the weight value helps the compensation of increasing the error at each iteration of reconstruction.

Although the extended height of the FOV can well reduce the accumulated error on the longitudinal plane, the capability of compensation still depends on accurate extrapolation in the extended height area of the projection images. Generally, accurate extrapolation is difficult to synthesize the lost data in the projection images. Although many techniques have attempted to simulate and estimate the lost data in the projections, the errors in the projection images still remain and are increased when fast iterative reconstruction has been run for many iterations. The error from inaccurate extrapolation is expanded from outside to inside the FOV, and that causes the MPE to diverge. Hence, the extended height of the FOV and projections help to mitigate the accumulated error expanding into the areas inside the FOV. For instance, the artifacts in the longitudinal plane inside the entire FOV with the proposed method can be enhanced better than those of the extension method only in the axial plane [13] as the noise is reduced as shown in Fig. 8 (d).

The acceleration techniques have been implemented in iterative reconstruction to reduce the reconstruction time by speeding up the convergence. However, such techniques have a serious effect on the accumulated error. The faster the convergence of iterative reconstruction is accelerated, the more the accumulated error in the reconstructed images is increased. The OS-10 and NES-10, which are the commonly used acceleration techniques in iterative reconstruction, were evaluated for the accumulated error after applying the proposed truncation effect reduction. Both techniques with the proposed method show decreasing in the accumulated error, while those without the proposed method show the increasing errors. The proposed truncation effect reduction compensates a large difference between the incomplete measurement and calculated forward projection as the extension of the entire FOV and noise regularization outside the FOV. However, the MPE of NES-10 diverges before OS-10 does. Divergence of the MPE is caused by the rapid accumulated errors from many subiterations and momentum weights [21]. The reconstructed images using NES in equation (3) are performed by the weight and summation of the momentum to achieve fast convergence, but the error while processing is always accumulated. In addition, increasing a number of subsets on both OS and NES also affects the rapid divergence [21]. Therefore, image quality evaluation and parameters of acceleration techniques in fast iterative reconstruction should be considered together for suitable solutions.

In low radiation dose acquisition, the soft tissues with low contrast often pose a challenge in discrimination of details in a noisy image. The ability of the proposed method to mitigate the noise substantially benefits the visualization images of soft tissues, such as the brain. The image of the brain reconstructed from the proposed method is clearly visualized and easily discriminable. The CNR is greatly improved due to significant noise reduction. The proposed method is evaluated for the image quality of the ventricles, which are the chambers containing the cerebrospinal fluid in the brain and are critical for diagnosis of hydrocephalus and intraventricular hemorrhage [27]. The visualization of the ventricles is challenging in CBCT because of a relatively low contrast of the area. Interestingly, the ventricle images from the proposed method can be observed much clearer compared to those from FBP having the same radiation dose. Here, the radiation dose (CTDI) of the CBCT data is only 5 mGy as compared to 70 mGy of a conventional fan-beam CT.

Even though our proposed method uses fast iterative reconstruction, the processing time of PL-C algorithm is still increased when the truncation effect reduction has been applied. The expected processing time of the PL-C algorithm with the proposed method is optimized by varying the parameters of the acceleration technique including the number of iterations, and the size of extended FOV based on acceptable image quality as 6 minutes with the proposed method using OS-10 and 20 iterations. Although another study [13] handled the processing time better than the proposed method, it did not mitigate the artifacts in the longitudinal plane of the FOV. The proposed method is able to compromise both image quality and processing time. Nevertheless, the proposed method can achieve good image quality in the reconstructed images inside the entire FOV in exchange for a considerable amount of the computational resources, including the GPU memory and processing time. The performance of the proposed method can be improved by finding an advanced technique to iterative reconstruction to

reduce the accumulated error outside the FOV, so that the extension of the FOV can be handled and the GPU memory and processing time can be reduced.

Conclusions

In this work, we proposed the truncation effect reduction for fast iterative reconstruction in CBCT imaging due to truncated data or incomplete projection images acquired from a CBCT scanner. Our proposed work extended the size of the FOV and the height of projection images, including the modified smoothness parameter β to zero outside the FOV for reconstruction. Here, fast iterative reconstruction used the PL-C algorithm with the acceleration techniques of the ordered subset and Nesterov's momentum weight techniques. The results of the head phantom and the human head data from the proposed method showed the significant decrease of the artifacts and the improvements on achieved image quality. The CNR of the soft-tissue images with the proposed method was distinctly improved by the increased contrast and the decreased noise. Visualization of the ventricle and soft-tissue images from the proposed method can be easily observed even with the very low radiation dose. Therefore, our proposed work has satisfactory performance to reduce the truncation effect in the CBCT reconstructed images and enhance soft-tissue imaging.

Abbreviations

CBCT: Cone-beam computed tomography; FPD: Flat-panel detector; FOV: Field of view; FBP: Filtered back projection; IR: Iterative reconstruction; PL-C: Modified convex algorithm with additional penalized likelihood estimation; DSD: Distance from a source to a detector; DSO: Distance from a source to an object; CTDI: Computed tomography dose index; GPU: Graphic processing unit; OS: Ordered subsets; NES: Nesterov; MPE: Mean-percentage-error; ROI: Region of interest; CNR: Contrast-to-noise ratio.

Acknowledgments

The authors would like to thank the Faculty of Medicine, Prince of Songkla University for research funding and feed-backs, and the Medical Imaging System Research Team, Assistive Technology and Medical Devices Research Center, National Science and Technology Development Agency for the CBCT prototype. We also thank Nattawut Sinsuebphon, Ph.D. for his review of the manuscript.

Authors' contributions

SA and SST conceived and designed this study. SA developed the algorithm and collected data for the experiment. SST contributed to analysis and evaluation. SA drafted the manuscript. SST critically revised the manuscript. PP and PT contributed to the design of the study. All authors read and approved the final manuscript.

Availability of data and material

The datasets generated and/or analysed during the current study are not publicly available, but are available from the corresponding author on reasonable request.

Ethics approval and consent to participate

Not applicable.

Consent for publication

Not applicable.

Competing interests

The authors declare that they have no competing interests.

Author details

[1]Faculty of Medicine, Price of Songkla University, Songkhla, Thailand. [2]Medical Imaging System Research Team, Assistive Technology and Medical Devices Research Center, National Science and Technology Development Agency, Pathum Thani, Thailand. [3]National Science and Technology Development Agency, Pathum Thani, Thailand.

References

1. Kalender WA, Kyriakou Y. Flat-detector computed tomography (FD-CT). European Radiology. 2007;17:2767-2779. doi:10.1007/s00330-007-0651-9.
2. Rumboldt Z, Huda W, All JW. Review of portable CT with assessment of a dedicated head CT scanner. AJNR Am J Neuroradiol. 2009; 30:1630-6. doi:10.3174/ajnr.A1603.
3. Xu J, Sisniega A, Zbijewski W, Dang H, Stayman JW, Mow M, Wang X, Foos DH, Koliatsos VE, Aygun N, Siewerdsen JH. Technical assessment of a prototype cone-beam CT system for imaging of acute intracranial hemorrhage. Med Phys. 2016;43:5745. doi:10.1118/1.4963220.
4. Dang H, Stayman JW, Sisniega A, Xu J, Zbijewski W, Wang X, Foos DH, Aygun N, Koliatsos VE, Siewerdsen JH. Statistical reconstruction for cone-beam CT with a post-artifact-correction noise model: application to high-quality head imaging. Phys Med Biol. 2015;60:6153-75. doi:10.1088/0031-9155/60/16/6153.
5. Thongvigitmanee SS, Aootaphao S, Thanasupsombat C, Kiang-ia A, Narkbuakaew W, Wangkaoom K, Junhunee P, Laohawiriyakamol S, Puttawibul P, Thajchayapong P. Cone-beam CT for breast specimens in surgery: the phantom study. IEEE Nuclear Science Symposium and Medical Imaging Conference. 2018; doi:10.1109/NSSMIC.2018.8824590.
6. Ohnesorge B, Flohr T, Schwarz K, Heiken JP, Bae KT. Efficient correction for CT image artifacts caused by objects extending outside the scan field of view. Med Phys. 2000;27:39-46. doi:10.1118/1.598855.
7. Hsieh J, Molthen RC, Dawson CA, Johnson RH. An iterative approach to the beam hardening correction in cone beam CT. Med Phys. 2000;27:23-9. doi:10.1118/1.598853.
8. Hsieh J, Chao E, Thibault J, Grekowicz B, Horst A, McOlash S, Myers TJ. A novel reconstruction algorithm to extend the CT scan field-of-view. Med Phys. 2004;31:2385-91. doi:10.1118/1.1776673.
9. Kyriakou Y, Kalender WA. X-ray scatter data for flat panel detector CT. Phys Med. 2007; 23:3-15. doi:10.1016/j.ejmp.2006.12.004.
10. Reitz I, Hesse BM, Nill S, Tucking T, Oelfke U. Enhancement of image quality with a fast iterative scatter and beam hardening correction method for kV CBCT. Med Phys. 2009;19:158-72. doi:10.1016/j.zemedi.2009.03.001.
11. Zhang X, Uneri A, Stayman JW, Zygourakis CC, Lo S-FL, Theodore N, Siewerdsen JH. Known-component 3D image reconstruction for improved intraoperative imaging in spine surgery: A clinical pilot study. Med Phys. 2019;46:3483-3495. doi:10.1002/mp.13652.
12. Maltz JS, Bose S, Shukla HP, Bani-Hashemi AR. CT truncation artefact removal using water-equivalent thicknesses derived from truncated projection data. Annu Int Conf IEEE Eng Med Biol Soc. 2007;2007:2907-11. doi:10.1109/IEMBS.2007.4352937.
13. Dang H, Stayman JW, Sisniega A, Zbijewski W, Xu J, Wang X, Foos DH, Aygun N, Koliatsos VE, Siewerdsen JH. Multi-resolution statistical image reconstruction for mitigation of truncation effect: application to cone-beam CT of the head. Phys Med Biol. 2017;62:539-559. doi:10.1088/1361-6560/aa52b8.

14. Huber PJ. Robust Statistics. New York: Wiley; 1981. doi:10.1007/978-3-642-04898-2_594.
15. Lange K, Carson R. EM reconstruction algorithms for emission and transmission tomography. J Comput Assist Tomogr.1984;8:306-16. https://pubmed.ncbi.nlm.nih.gov/6608535/.
16. Kamphuis C, Beekman FJ. Accelerated iterative transmission CT reconstruction using an ordered subsets convex algorithm. IEEE Trans. on Medical Imaging. 1998;17:1101-1105. doi:10.1109/42.746730.
17. Fessler JA. Statistical image reconstruction methods for transmission tomograph in handbook of medical imaging. Bellingham: SPIE Press. 2000. doi:10.1117/3.831079.ch1.
18. Aootaphao S, Pintavirooj C, Sotthivirat S. Penalized-likelihood reconstruction for metal artifact reduction in cone-beam CT. Annu Int Conf IEEE Eng Med Biol Soc. 2008;2088:2733-6. doi:10.1109/IEMBS.2008.4649767.
19. Kim D, Fessler JA. Ordered subsets acceleration using relaxed momentum for x-ray CT image reconstruction. IEEE Nuclear Science Symposium and Medical Imaging Conference. 2013; doi:10.1109/NSSMIC.2013.6829298.
20. Kim D, Ramani S, Fessler JA. Combining ordered subsets and momentum for accelerated x-ray CT image reconstruction. IEEE Trans Med Imaging. 2015;34:167-78. doi:10.1109/TMI.2014.2350962.
21. Wang AS, Stayman JW, Otake Y, Vogt S, Kleinszig G, Siewerdsen JH. Accelerated statistical reconstruction for C-arm cone-beam CT using Nesterov's method. Med Phys. 2015;42:2699-708. doi:10.1118/1.4914378.
22. Feldkamp LA, Davis LC, Kress JW. Practical cone-beam algorithm. J. Opt. Soc. Am. A. 1984;1:612-619. doi:10.1364/JOSAA.1.000612.
23. Kak AC, Slaney M. Principles of Computerized Tomographic Imaging. New York: IEEE Press. 1988. doi:10.1137/1.9780898719277.
24. Aootaphao S, Thongvigitmanee SS, Rajruangrabin J, Junhunee P, Thajchayapong P. Experiment-based scatter correction for cone-beam computed tomography using the statistical method. Annu Int Conf IEEE Eng Med Biol Soc. 2013. doi:10.1109/EMBC.2013.6610692.
25. Aootaphao S, Thongvigitmanee SS, Rajruangrabin J, Thanasupsombat C, Srivongsa T, Thajchayapong P. X-ray scatter correction on soft tissue images for portable cone beam CT. Biomed Res Int. 2016;2016:3262795. doi:10.1155/2016/3262795.
26. Kim D, Pal D, Thibault J-B, Fessler JA. Accelerating ordered subsets image reconstruction for x-ray CT using spatially nonuniform optimization transfer. IEEE Trans Med Imaging. 2013;32:1965-78. doi:10.1109/TMI.2013.2266898.
27. Wu P, Sisniega A, Stayman JW, Zbijewski W, Foos D, Wang X, Khanna N, Aygun, N, Stevens RD, Siewerdsen JH. Cone-beam CT for imaging of the head/brain: development and assessment of scanner prototype and reconstruction algorithms. Med Phys. 2020; 47:2392-2407. doi:10.1002/mp.14124.